Flow visualization around a flapping-wing micro air vehicle in free flight

Del Estal Herrero, Alex; Perçin, Mustafa; Karasek, Matej; van Oudheusden, Bas

DOI
10.3929/ethz-b-000279207

Publication date
2018

Document Version
Final published version

Published in
Proceedings 18th International Symposium on Flow Visualization

FLOW VISUALIZATION AROUND A FLAPPING-WING MICRO AIR VEHICLE IN FREE FLIGHT

Alejandro del Estal Herrero[1], Mustafa Percin[1,2], Matej Karasek[1] and Bas W. van Oudheusden[1,c]

[1]Department of Aerospace Engineering, Delft University of Technology, Delft, The Netherlands
[2]Department of Aerospace Engineering, Middle East Technical University, Ankara, Turkey
[c]Corresponding author: email: b.w.vanoudheusden@tudelft.nl

KEYWORDS: flow visualization, flapping-wings, micro air vehicles, Particle Image Velocimetry

ABSTRACT: *Flow visualizations have been performed on a free flying flapping-wing Micro Air Vehicle (MAV), using a large-scale particle image velocimetry (PIV) approach. The PIV method involves the use of helium filled soap bubbles (HFSB) as tracer particles. HFSB scatter light with much higher intensity than regular seeding particles and comparable to that reflected off the flexible flapping wings. This enables flow field visualization to be achieved also close to the flapping wings, in contrast to previous PIV experiments with regular seeding. Unlike previous tethered wind tunnel measurements in which the vehicle is fixed relative to the measurement setup, the MAV now flies through the measurement area. In this way, the experiment captures the actual flow field of the MAV in free flight, allowing the true asymmetric nature of the flow to be appreciated. Measurements were performed for two different orientations of the light sheet with respect to the flight direction. In the first configuration, the light sheet is parallel to the flight direction and visualizes a streamwise plane that intersects the MAV wings at a specific spanwise position. In the second configuration, the illumination plane is normal to the flight direction and visualizes the flow as the MAV passes through the light sheet.*

1 Introduction

The development of flapping-wing Micro Air Vehicles (MAVs) often draws inspiration from nature, like birds, bats or insects [1][2][3][4], but simply copying nature cannot be expected to lead to optimized MAV designs. Understanding the aerodynamic working mechanisms of these bio-inspired designs is challenging due to the complexity of the flow around the flapping wings [5] and has been a subject of extensive study. Out of practical considerations, most experimental studies on actual MAV platforms or prototypes are performed in a constrained configuration, where the MAV is "tethered" by mounting it in a fixed position relative to the flow visualization setup. Tests may represent either a hover configuration by conducting experiments in a stagnant environment [6][7] or mimic forward flight by using a wind tunnel [8][9], at settings corresponding to the actual flight envelope. However, the physical restriction imposed on the flapping MAV inhibits the dynamic body modes that occur in real flight, which may also affect the aerodynamic behaviour [10].

The MAV used in the current tests is the DelFly II (henceforth called DelFly for simplicity) [3], for which tethered experiments have been previously performed in hovering [11][12] and symmetric forward flight (zero pitch) [9] configuration. These configurations both result in symmetrical flow patterns around the wings, which is not representative of true forward flight, where an appreciable forward velocity is combined with a high pitch angle. Tethered flow visualization experiments were carried out on a different DelFly version at relatively small pitch angles [13], whereas [14] reports on preliminary results of a setup intended to enable free-flight wake visualization by controlling the MAV position in the exit of a large wind tunnel. In line with this interest, the particular objective of the current study is to visualize the unsteady flow structures around the MAV in actual forward flight. For this the MAV was guided by an automatic flight control system, similar to [14], in a trajectory through the test space in which flow visualization was achieved with planar particle image velocimetry (PIV) using helium-filled soap bubbles (HFSB) as tracer particles [15].

2 Methods

2.1 The DelFly MAV

The DelFly MAV is a four-wing flapping MAV with wing pairs on either side of the vehicle that are set at a dihedral angle of 12° and actuated in counter-phase (see Figs. 1 and 2). The total wing span is 280 mm and the maximum stroke angle ϕ is 87°. The wings are constructed from 15 µm thick transparent Mylar foil, with carbon-fiber leading edge spars and wing stiffeners completing the wing structure. The leading edge spars are driven in a periodic flapping motion, during which the wing surfaces undergo appreciable passive deformation [11][16]. Figure 2 explains the wing kinematics nomenclature based on the leading edge motion, with the *outstroke* being the phase in the flapping cycle where the wings move away from each other, while the *instroke* is the phase where they move towards each other. It is to be noted that as a result of the wing flexibility, the wing surface motion displays an appreciable delay with respect to that of the driven leading edge.

The mass of the DelFly model used in the experiments is approximately 25 grams, and the total vehicle length is about 215 mm. The tail assembly has a span of 170 mm and is constructed from 2 mm thick Depron polystyrene sheet and was painted black to reduce light reflections. The flight speed during the present tests is around 1 m/s, with the pitch angle and the flapping frequency being around 60° and 14 Hz, respectively.

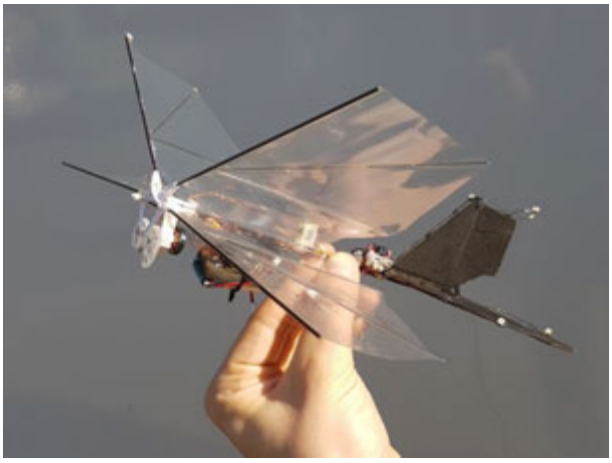

Fig. 1. The DelFly MAV used in the experiments.

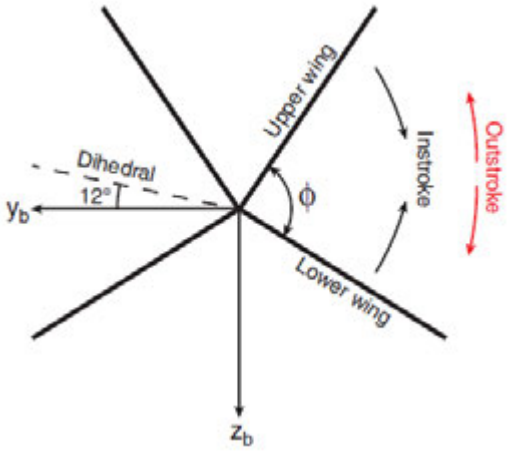

Fig. 2. Wing motion definitions.

2.2 The flight control system

The automatic control system used for this free-flight investigation is similar to the one used in [14], consisting of an optical motion tracking system and an onboard autopilot system. The tracking system is comprised of 24 cameras (OptiTrack Flex 13), which were positioned on the ceiling of the flight area for tracking the 7 infrared LED markers placed on the DelFly MAV (body, tail, wing and control surfaces). The online position and orientation information obtained by the tracking system is fed via a wireless link (WiFi) to the onboard autopilot system (Lisa/S autopilot [17] with Paparazzi UAV software) that guides the DelFly in a prescribed trajectory through the measurement area.

The DelFly vehicle was programmed to follow an oval trajectory, consisting of two half circles of 4 m in diameter with two 3 m long straight segments in between (see Fig. 3). The PIV measurement area was located approximately in the middle of one of the straight segments, such that the vehicle would have time to recover to a steady flight state after the turn and its trajectory would not interfere with the camera setup. Given the forward speed of 1 m/s, the vehicle crossed the test

section approximately every 15 seconds. Since the trajectory following was not perfect due to slightly worse tracking under the net covering the test section, as well as due to external disturbances such as drafts, an operator was monitoring the lateral position error and could decide to redo the experiment during the next pass if needed. The measurement itself was triggered by the operator prior to the moment when the vehicle would enter the test section (cf. Fig. 4). This would also light up additional LED markers, detected by the motion tracking system, which was used to synchronize the motion tracking data with the PIV dataset. In this way, the vehicle position, orientation, and the wing stroke angle corresponding to each PIV frame could be determined.

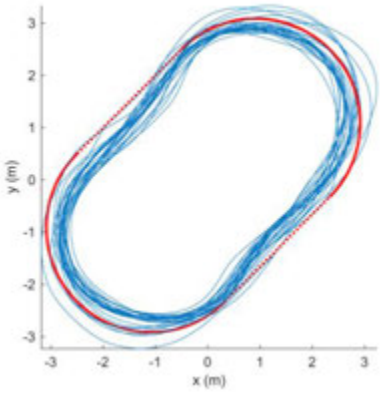

Fig. 3. The nominal (red) and realized (blue) flight trajectories.

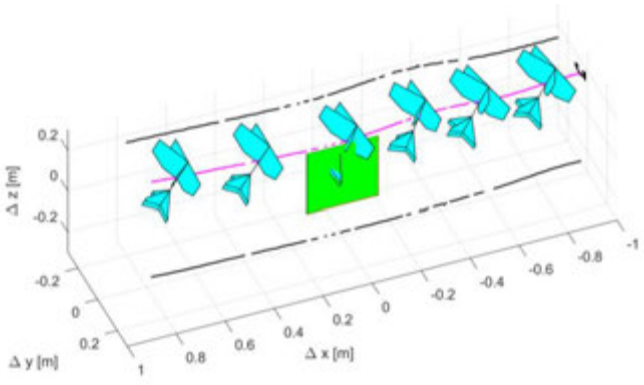

Fig. 4. The DelFly crossing the measurement area (the purple line indicates the center-of-gravity path).

2.3 The Particle Image Velocimetry (PIV) procedure

The employed PIV technique uses nearly-neutrally-buoyant helium filled soap bubbles (HFSB; approximate size 300 μm) as tracer particles to allow a large field of view to be measured [15], while at the same time mitigating the effect of the laser light reflections from the flapping wings. As the bubbles scatter significantly more light than micron-sized droplets, the ratio of particle light intensity to the parasite wing reflection intensity is increased. This enables flow field visualization to be achieved also relatively close to the wings, in contrast to previous PIV experiments in which regular PIV seeding was used.

The experimental procedure is illustrated in Figs. 4 and 5. The test area was filled with the helium-filled soap bubbles prior to the PIV measurements and enclosed at the sides and the top with a fine-maze net to contain the bubbles so as to maintain a sufficient tracer concentration. A high-speed Nd:YAG laser (Mesa-PIV at a wavelength of 532 nm and 18 mJ pulse energy) was employed to provide illumination from below in the form of a vertically projected laser light sheet. Two visualization configurations were used, differing in the orientation of the light sheet with respect to the MAV flight path. Firstly, planar (2C) PIV measurements were performed in a streamwise (i.e., chordwise) aligned plane. For this purpose, a single high-speed camera (Photron Fastcam SA-1.1) was employed to record images of the HFSB tracers. Subsequently, two high-speed cameras in a stereoscopic configuration were used to obtain all three velocity components in a spanwise-aligned measurement plane capturing the flow field during the passage of the DelFly model. The two imaging configurations are illustrated in the schematic in Fig. 5. In both cases, the field of view is approximately 350×350 mm^2 and the image recording rate 2 kHz, corresponding to approximately 140 images per flapping cycle. Time-series of single-frame images were interrogated with a final window size of 48×48 pixels with an overlap factor of 75%, yielding a vector resolution of 3.8 mm.

Fig. 5. Top view schematic of the test arrangement (left); setup for the stereoscopic PIV measurements (right).

3 Results

3.1 Streamwise planar flow visualizations

In the first measurement configuration the light sheet is oriented parallel to the flight direction (see also Fig. 4) and visualizes a streamwise plane that intersects the MAV wings at a specific spanwise position, which is determined by the lateral displacement of the flight path with respect to the light sheet. The latter proved difficult to control accurately, providing limited control over the spanwise position of the imaged measurement plane. Two useful datasets were obtained, corresponding to 45±4% (S1) and 63±3% (S2) of the half-span of the wings, respectively. The flight conditions were similar for both cases (flight speed 1.0±0.1 m/s, pitch angle 61°–62° and flapping frequency 13.5 Hz). At these conditions a full crossing of the field of view is performed in 0.35 seconds, which corresponds to approximately 5 flapping cycles, comprising a dataset of about 700 images.

Flow structures in a chordwise-oriented plane at approximately 45% of the semi-span (dataset S1) are shown in Fig. 7, covering one complete flapping cycle, with nondimensional time defined as $t^* = t/T$ ($T = 1/f$ being the flapping period) and $t^* = 0$ corresponding to the moment of the stroke direction reversal that marks the end of the instroke and the beginning of the outstroke. The position and cross-sectional shape of the two wings are clearly visible, and reflect the advancement of the MAV in the flight direction (i.e. towards the right) as time progresses. In the shaded area the illumination is obstructed by the tail surface, preventing meaningful measurements to be performed there. The white arrows indicate the relative motion of the wings with respect to each other, and it can be clearly seen that shortly after stroke reversal the wing flexibility results in an apparent rotation of the wings (see $t^* = 0.6$, a similar behavior occurs near $t^* = 0.1$). Also, in the early phase of the outstroke (see $t^* = 0.2$) the visualization gives clear evidence of the “clap-and-peel” effect [11][16], where the rear part of the wings remain connected during the first phase of the outstroke.

The visualizations give clear evidence that the flow conditions, under the combined effect of forward velocity, high pitch angle and wing flapping, result in asymmetric flow patterns being generated around the wings. For example, at $t^* = 0.4$, which is towards the end of the outstroke, the lower (= right) wing has a much more coherent leading-edge vortex (LEV) than the upper wing. This can be attributed to the smaller effective velocity of the upper (= left) wing due to the forward motion of the DelFly, which also decreases the effective angle of attack and mitigates the flow separation (compare the results of [13]). It may be hypothesized that in this phase most of the lift (vertical force, in y direction) is hence generated by the lower wing, whereas the upper wing mostly

accounts for the thrust (horizontal force, in the x direction). It can be further observed that towards the end of the instroke (t* = 1.0) the lower wing releases a large trailing-edge vortex (TEV) into the wake, which can also be observed at t* = 0.0. Most likely a TEV of opposite vorticity is released by the upper wing, but its signature is blocked by the laser shadow region of the tail.

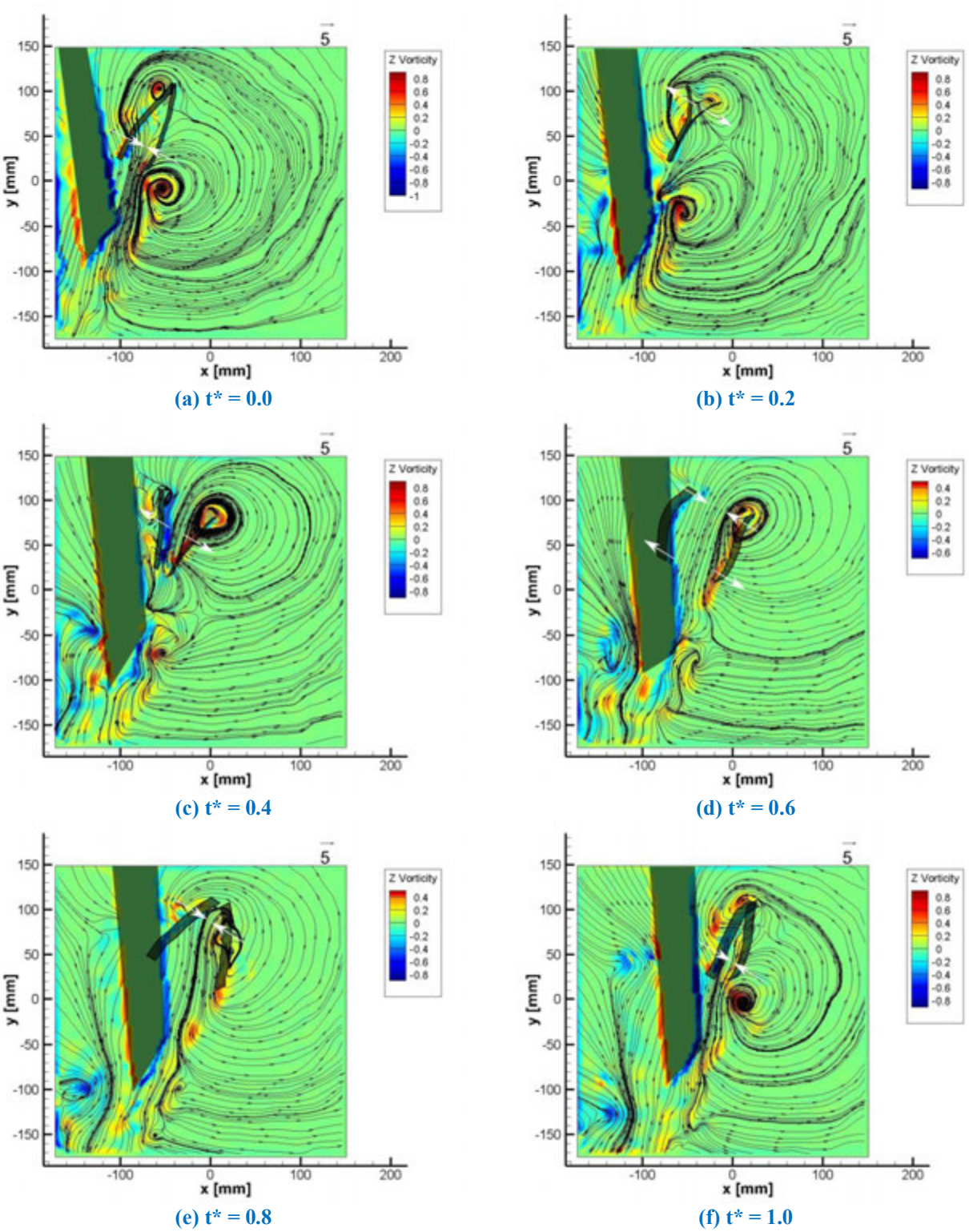

(a) t* = 0.0 (b) t* = 0.2

(c) t* = 0.4 (d) t* = 0.6

(e) t* = 0.8 (f) t* = 1.0

Fig. 6. Contours of out-of-plane vorticity and in-plane streamline patterns during one flapping sequence.

3.2 Analysis of the flow-induced effect of the flapping wings

In an effort to quantify the propulsive effect of the flapping wings, the relative acceleration of the flow is assessed on the basis of a momentum analysis, comparing the upstream and downstream conditions near the wings (constrained to the two dimensional flow data provided by the 2C PIV method). For this purpose, the flow velocity is monitored at two points in the flow field in relative position with respect to the MAV, denoted by the "inlet" and the "outlet", thus tentatively comparing the gap between the wings to a propulsive channel. These points are taken at the symmetry plane between the wings, slightly above the leading edge and under the trailing edge, respectively. Figure 8 shows the results for the flow velocity components at these two monitoring positions, for the available full flapping cycles for each experiment (three cycles for S1 and two cycles for S2), with the datasets synchronized at $t^* = 0$ for the onset of the outstroke. The solid lines indicate the actual variations over the individual cycles, while the dashed lines represent phase-averaged results, which verifies the periodicity of the results. It can be observed in Fig. 8a that for the inlet position the velocity variation is relatively small and displays in general a very periodic trend. Velocities are seen to decrease (i.c. become more negative) during the outstroke and to increase during the instroke, which is consistent with the induced flow generated near the wing leading edges in these phases of the flapping cycle. For the outlet position (Fig. 8b) much stronger variations occur, with a distinctly different pattern for the instroke and outstroke phases, especially regarding the vertical velocity component. During much of the outstroke the vertical velocity remains relatively small in magnitude, and that more so for the inboard location (S1) than for the outboard one (S2). This likely reflects the inhibition of the downward flow by the closure of the wing gap during the "fling phase" (compare Fig. 7b). Once this gap is opened (which occurs around $t^* = 0.4$) and also during the subsequent instroke, the vertical velocity reaches large negative values, indicating a strong downward flow. The horizontal velocity component shows less variation, which is likely due to the high pitch angle of the DelFly, apart from occasional peaks in the force signal that may be due to measurement uncertainty and the occurrence of vortices near the wing leading edges.

A second aspect of relevance for the performance of a flapping-wing MAV of the current configuration, being equipped with a conventional tail assembly, is how the flow conditions near the tail are affected by the strong periodic variations of the wake flow of the flapping wings. For this, an estimate is made of the flow conditions perceived by the tail, by taking into account the flow induced by the wings in combination with the forward flight speed. Next, the flow conditions are expressed in terms of the absolute velocity magnitude and the effective angle of attack relative to the plane of the horizontal tail surface (Fig. 9). Note that the S2 position (at 63% semi-wing span) corresponds approximately to the tip of the horizontal tail surface (which is at 61% of the semi-wing span), whereas the S1 position (at 45% semi-wing span) corresponds approximately to 75% of the tail semi-span. It is observed that over most of the flapping cycle, the absolute airspeed is quite high (between 3 and 5 m/s) compared to the flight speed (~ 1 m/s). For reference, this may be compared to the mean wing tip speed (~ 5 m/s) or the average induced speed estimated from actuator disk theory (ca 2.7 m/s). From the results shown in Fig. 9 it is perceived that during the outstroke the angle of attack is first positive and then negative, however, the airspeed remains relatively low during the outstroke. During the instroke, on the other hand, the airspeed is high, yet the angle of attack remains near zero.

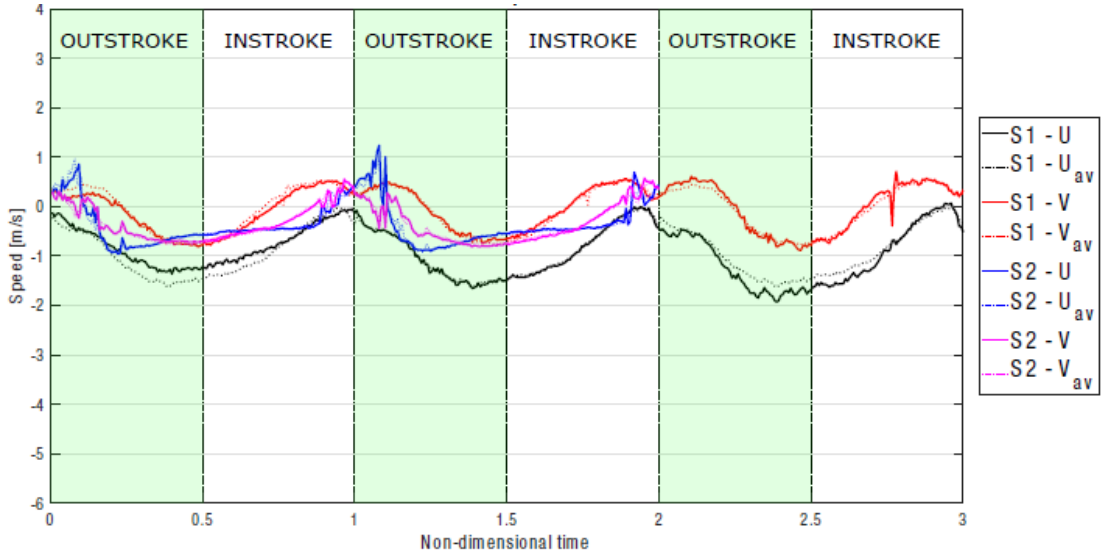

(a) inlet

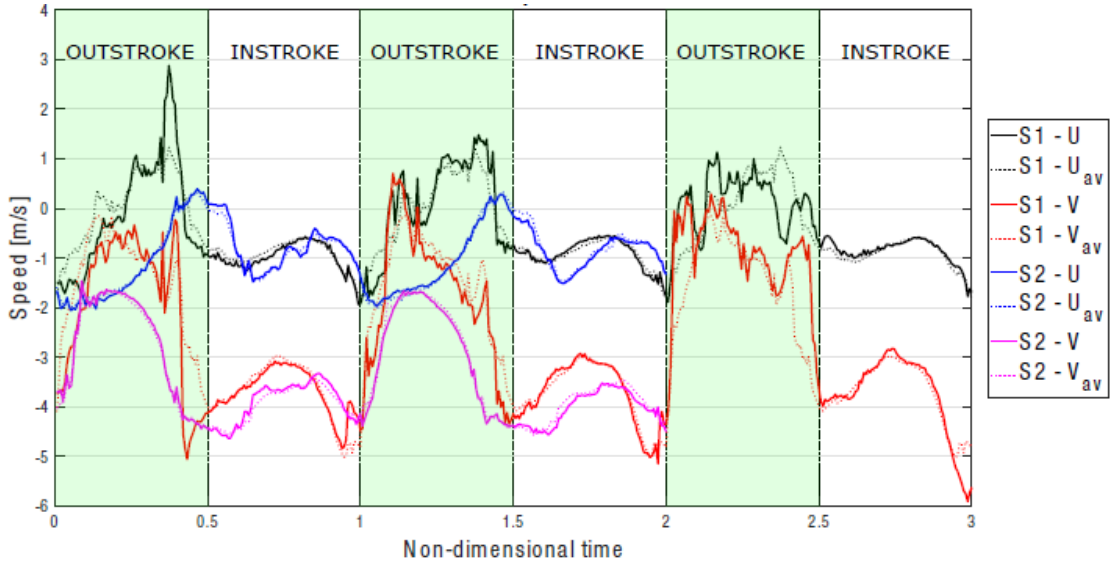

(b) outlet

Fig. 7. Evolution with non-dimensional time t* of the velocity around the DelFly for experiments (S1) and (S2) at different relative probe positions ("inlet" and "outlet"). U and V refer to the horizontal and V vertical speed, respectively. The dashed lines (subscript av) indicate the results averaged over the available flapping sequences.

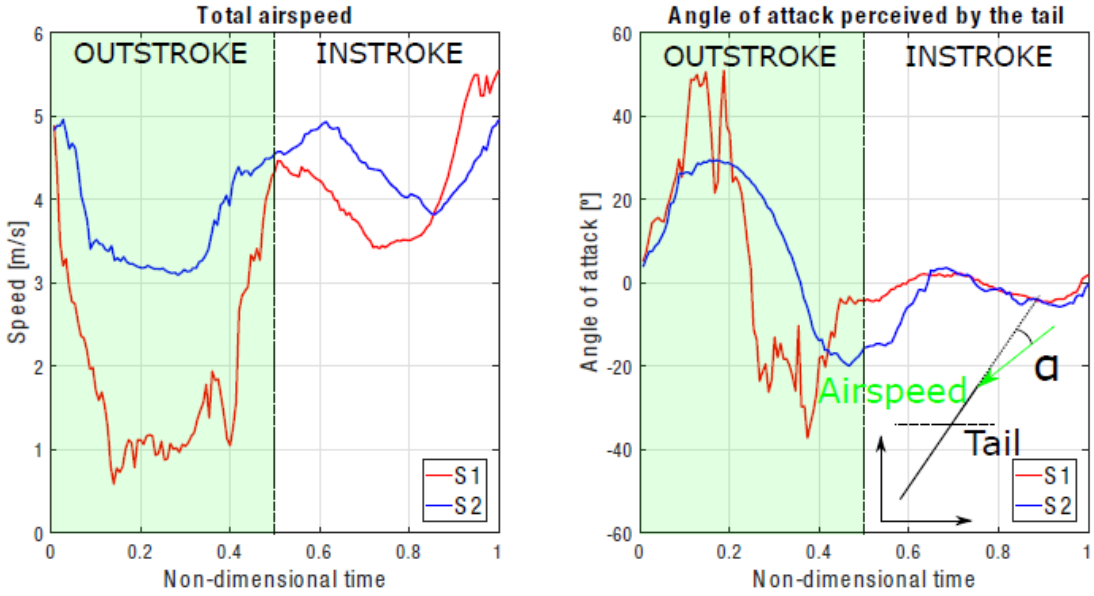

Fig. 8. Flow conditions perceived by the tail, for two different spanwise positions (S1: 45% and S2: 63% of semi-wing span).

3.3 Spanwise planar flow visualizations

In the second visualization configuration, the illumination plane is normal to the flight direction and visualizes the flow development as the MAV passes through the light sheet, which is captured by the stereoscopic PIV configuration (see Fig. 5). The practical aspects of this approach are simpler, as it is less sensitive to the precise lateral and vertical positioning of the flight path. However, the interpretation of the visualizations proved to be much more complex, as the flow structures that are observed in the measurement plane depend on both the position of the MAV with respect to the light sheet and the flapping phase of the wings, which is further complicated when the MAV crosses the plane with a yaw or sideslip angle. Therefore, removal of this ambiguity in the flow visualization would best be served by a true volumetric method, see e.g. [18].

Figure 10 shows results obtained for one of the passes, with the wings being at the end of the instroke. The image on the left displays virtual pathlines, which are generated by applying a time-filter algorithm (with a filter length of seven time steps) on the images captured by the Camera-1 of the stereoscopic configuration (see Fig. 5). This process enables visualization of prominent rotational flow structures, notably the tip vortices of the upper wings and the tail. Contours of out-of-plane vorticity (Fig. 10-right) also reveal the occurrence of wing root vortices, which have an opposite rotational direction compared to the tip vortices of the corresponding wings.

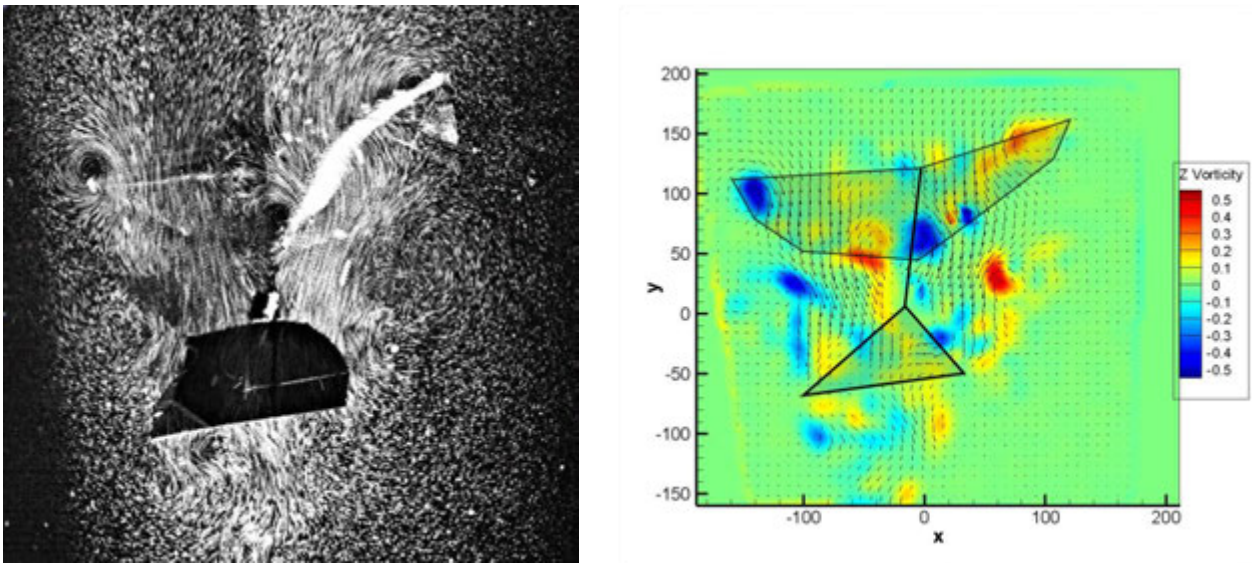

Fig. 9. Time-filtered stereoscopic-PIV image (left) and contours of out-of-plane vorticity in a spanwise-oriented plane (right) at the end of the instroke; DelFly model outline is indicative only.

4 Conclusion

Flow visualizations have been performed on a flapping-wing Micro Air Vehicle (MAV) in free flight, using a large-scale particle image velocimetry (PIV) approach. The PIV methodology involves the use of helium filled soap bubbles (HFSB). The results permit the identification of the different aerodynamic behavior of upper and lower wings in actual forward flight conditions, as well as the generation of streamwise vortices by wings and tail. The results were further used to estimate the flow conditions near the MAV tail, which is of relevance for the flight performance in terms of control and stability.

References

[1] Wood RJ. The first takeoff of a biologically inspired at-scale robotic insect. *IEEE Transactions on Robotics*, Vol. 24, pp. 341–347, 2008.

[2] Keennon M, Klingebiel K, Won H, Andriukov A. Development of the nano hummingbird: a tailless flapping wing micro air vehicle. AIAA 2012-0588, *50th AIAA Aerospace Sciences Meeting*, Nashville, USA, 9-12 Jan 2012.

[3] de Croon GCHE, Percin M, Remes BDW, Ruijsink R, de Wagter C. *The DelFly*. Springer, 2016.

[4] Ramezani A, Chung S-J, Hutchinson S. A biomimetic robotic platform to study flight specializations of bats. *Science Robotics*, Vol.2, eaal2505, 2017.

[5] Sane SP. The aerodynamics of insect flight. *Journal of Experimental Biology*, Vol.206, pp. 4191-4208, 2003.

[6] Nguyen QV, Truong QT, Park HC, Goo NS, Byun D. Measurement of force produced by an insect-mimicking flapping-wing system. *Journal of Bionic Engineering*, Vol.7, pp. 94–102, 2010.

[7] Lin C-S, Hwu C, Young W-B. The thrust and lift of an ornithopter's membrane wings with simple flapping motion. *Aerospace Science & Technology*, Vol.10, pp. 111–119, 2006.

[8] Lee J-S, Han J-H. Experimental study on the flight dynamics of a bioinspired ornithopter: free flight testing and wind-tunnel testing. *Smart Materials and Structures*, Vol.21, pp. 094023, 2012.

[9] Percin M, van Oudheusden B, Eisma H, Remes B. Three-dimensional vortex wake structure of a flapping-wing micro aerial vehicle in forward-flight configuration. *Experiments in Fluids*, Vol.55, pp. 1–16, 2014.

[10] Caetano JV, Percin M, van Oudheusden BW, Remes B, de Wagter C, de Croon GCHE, de Visser CC. Error analysis and assessment of unsteady forces acting on a flapping wing micro air vehicle: free flight versus wind-tunnel experimental methods. *Bioinspiration & Biomimetics*, Vol.10, 056004, 2015.

[11] De Clercq KME, de Kat R, Remes B, van Oudheusden BW, Bijl H: Aerodynamic experiments on DelFly II: unsteady lift enhancement, *International Journal of Micro Air Vehicles*, Vol.1, pp. 255-262, 2009.

[12] Percin M, van Oudheusden BW, Remes B: Flow structures around a flapping-wing micro air vehicle performing a clap-and-peel motion, *AIAA Journal*, Vol.55, pp. 1251-1264, 2017.

[13] Deng S, van Oudheusden BW. Wake structure visualization of a flapping-wing micro-air-vehicle in forward flight. *Aerospace Science & Technology*, Vol.50, pp. 204-211, 2016.

[14] Karasek M, Percin M, Cunis T, van Oudheusden BW, De Wagter C, Remes BDW, de Croon GCHE. First free-flight flow visualisation of a flapping-wing robot, https://arxiv.org/abs/1612.07645, 2016.

[15] Scarano F, Ghaemi S, Caridi GCA, Bosbach J, Dierksheide U, Sciacchitano A. On the use of helium-filled soap bubbles for large-scale tomographic PIV in wind tunnel experiments. *Experiments in Fluids*, Vol.56, 42, 2015.

[16] Percin M, van Oudheusden BW, de Croon GCHE, Remes B. Force generation and wing deformation characteristics of a flapping-wing micro air vehicle 'DelFly II' in hovering flight, *Bioinspiration & Biomimetics*, vol.11, 036014, 2016.

[17] Remes BDW, Esden-Tempski P, van Tienen F, Smeur E, De Wagter C, de Croon, GCHE. Lisa-S 2.8g autopilot for GPS-based flight of MAVs. *IMAV 2014: International Micro Air Vehicle Conference and Competition 2014*, Delft, The Netherlands, August 2014.

[18] Martínez Gallar B, van Oudheusden BW, Sciacchitano A, Karasek M. Large-scale flow visualization of a flapping-wing micro air vehicle, *18th International Symposium on Flow Visualization*, Zurich, Switzerland, 26-29June 2018.

Copyright Statement